Time Resolved Beam Divergence from a Copper Vapor Laser with Unstable Resonator

David W. Coutts, *Member, IEEE*

Abstract— **The temporal evolution of the far-field intensity distribution (and hence beam divergence) for the output of a CVL operating with both on-axis and off-axis unstable resonators is investigated in detail. The CVL output pulse consists of several temporally resolved components, where each successive component has lower divergence approaching the diffraction limit. A comprehensive model for the divergence of each temporal component from a CVL operating with a variety of unstable resonators is presented. In this model the resonator controls the output divergence by imposing geometric constraints on the propagation of spontaneous emission on repeated round-trips through the unstable resonator equivalent lensguide. Effects of resonator asymmetry and radial gain variations on the far-field intensity distribution (and hence divergence) are evaluated. Experimental measurements of the temporal evolution of output divergence from a CVL operating with both on-axis and off-axis unstable resonators and for a variety of excitation conditions are also presented. For CVL operation at high pulse repetition frequency the ASE at the start of the laser pulse has an annular profile. This annular gain distribution is found to modify the output far-field intensity distribution of the earlier temporal components of the laser pulse. For on-axis unstable resonators these components are found to have annular far-field intensity distributions, whereas for off-axis unstable resonators they have greatly reduced but anisotropic divergence.**

I. Introduction

COPPER vapor lasers (CVL's) are efficient (up to 1%) high average power (tens to hundreds of watts), high pulse repetition rate (4–20 kHz) laser sources in the green (510.6 nm) and yellow (578.2 nm). Many important new applications including micro machining [1], nonlinear frequency conversion [2] and pumping Ti : Sapphire lasers [3], require a CVL with very low or well characterised beam divergence.

The CVL is characterised by having exceptionally high small-signal gain (up to 25%/cm), short gain duration (typically less than five resonator round-trips), and large gain volume. Due to the short gain duration and intense ASE seeding of the output, there is insufficient time for the production of resonator modes by requiring the intracavity field to conform to *round-trip* boundary conditions, rather the resonator acts to control the formation of output principally by imposing geometric constraints on the propagation of the initial ASE seed through successive round-trips. In this way the CVL effectively operates as a multipass amplifier for the ASE seed, and as such, it is misleading to describe the output in terms of resonator modes.

Unstable resonators provide greater spatial control over the round-trip propagation of intracavity radiation than the plane-plane resonators typically employed with CVL's. With their greater control over the intracavity radiation, high magnification (M $\sim$ 15 to 100) unstable resonators can yield high beam quality (low divergence) output from CVL's [4], [5]. However, even with an unstable resonator, the divergence evolves significantly during the laser pulse, falling from an initially high value of several milliradian (hundreds of times the diffraction-limit), down to near the diffraction-limit at the end of the pulse [5]. To date there have been few reports of measurement of the temporal development of CVL beam divergence [5]–[8], and few attempts to calculate the evolution of beam quality from such lasers [9]–[11]. In these reports only on-axis resonators were considered; however it has been observed by several authors [12], [13] that when there are large radial variations in the onset of gain in CVL's, significant improvements in low divergence output power can be achieved by changing from the conventional on-axis unstable resonator to an off-axis unstable resonator.

In this paper, a ray-tracing model is described which enables the *far-field intensity distribution* (and hence divergence) of each component of the CVL output to be calculated directly for a CVL operating with both on-axis and off-axis unstable resonators, and for both near-uniform and radially varying gain. Detailed experimental measurements of the far-field intensity distribution at each stage of the laser pulse are presented for all these cases. The model is sufficient to enable the prediction of far-field intensity profiles which accurately agree with the measured profiles.

II. Modelling Output Divergence

Previous theoretical investigations into the output divergence for CVL's fitted with unstable resonators have been directed towards calculating the time required to establish output with diffraction-limited divergence [14]–[16], [5]. These calculations have been based on the propagation of demagnifying and magnifying waves within the unstable resonator, where the time to establish diffraction-limited output divergence is derived from the time required to transform a demagnifying wave into a magnifying wave. No consideration has been given to the spatial characteristics of the output produced during the pulse prior to the formation of a diffraction-limited beam. Since a significant fraction (sometimes all) of the CVL output

Manuscript received May 4, 1994; revised August 10, 1994. This work was supported by the Australian Research Council and Macquarie University.

The author was with the Centre for Lasers and Applications, Macquarie University, NSW 2109, Australia. He is now with the Department of Atomic and Laser Physics, Clarendon Laboratory, University of Oxford, Parks Road, Oxford OX1 3PU, U.K.

IEEE Log Number 9407806.

pulse occurs prior to the establishment of diffraction-limited output, it is very important to be able to evaluate the beam divergence at each stage of the laser pulse.

Recent measurements [8] have established that the output of a CVL fitted with a conventional high-magnification positive-branch unstable resonator consists of a series of discrete temporal components (usually four or five) with each successive component having lower divergence than the previous one; the divergence thus falls in a stepwise fashion during the laser pulse. These temporal components have been demonstrated to be derived from the propagation of an initial burst of amplified spontaneous emission on repeated round-trips within the unstable resonator, where propagation through each successive round-trip gives rise to a separate temporal component in the CVL output pulse [17]. The different temporal components observed can be labelled the two-pass, four-pass, six-pass and eight-pass outputs according to the number of times radiation from the initial spontaneous emission seed has passed through the gain medium before exiting the unstable resonator past the spot-reflector output-coupler. These components therefore correspond to light that has made up to one, two, three or four round-trips within the unstable resonator. (Under some circumstances, usually corresponding to low magnification unstable resonators, components comprising odd-number of passes are also observed, however they usually contain only a small fraction of the total power and each odd-pass component has divergence characteristics very similar to the even-pass component that immediately follows it.)

In order to model the divergence characteristics of each temporal component of the CVL output, an unfolded resonator approach may be used [18]. In this approach, the propagation of spontaneous emission on repeated "round-trips" of the unfolded resonator lensguide equivalent is examined. Note that the temporal evolution of the transverse coherence radius has also been modelled in this manner by several Authors [9]–[11], however the transverse coherence radius, being a single parameter, can not fully characterise CVL beam quality, particularly where the far-field intensity distribution is not simple in structure. In this paper, the effects of the resonator geometric constraints on the formation of each temporal component of the output are determined by examining the propagation of rays from each point on the seed (the initial burst of amplified spontaneous emission) through the corresponding number of stages of the unfolded lensguide equivalent of the unstable resonator. With this approach, each temporal component of the output beam is described as a collection of rays where both the propagation angle and spatial position of each ray comprising the output beam are known. The *far-field intensity distribution* (and hence divergence) for each temporal component is then calculated directly by examining the subsequent propagation (i.e., after leaving the resonator) of the rays comprising that component.

For the purposes of the model the CVL gain may be assumed to be nearly uniform and saturated at all times except in the first few ns of the gain period when the seed is formed [17]. Spatial variations in the gain are therefore included only in the description of the seed. This enables a model based on an unloaded resonator (resonator without gain) approach to be adopted, which is adequate to predict the far-field intensity profiles.

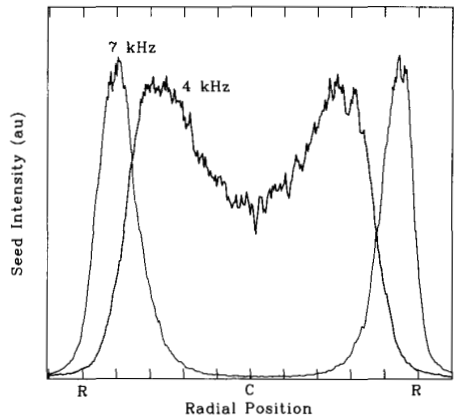

Fig. 1. Measured seed intensity profiles for the CVL operating at 4 kHz and 7 kHz.

The seed radiation consists of the incoherent spontaneous emission at the two CVL wavelengths which, on propagation on repeated round-trips through the resonator, gives rise to all the observable output. The principal contribution to the seed radiation consists of spontaneous emission occurring at the output coupler end of the laser tube which propagates initially towards the high reflector, as this radiation sees the greatest gain length before exiting the resonator at the output coupler. Convolution of the spontaneous emission radial profile with the unsaturated gain profile at the start of the pulse gives rise to an effective intensity profile for the seed radiation. Measurements of the effective seed intensity [17] showed that for some CVL operating conditions (usually corresponding to low prf operation) the seed radiation intensity profile varies by less than 50% across most of the tube aperture. However, for large bore CVL's (tube diameters over 40 mm) and for operation at elevated prf, the seed radiation intensity is greatly depleted on the tube axis (intensity on axis $<2\%$ that at the walls). Measured seed intensity profiles for operation of the same CVL (25 mm tube diameter) at 4 kHz and 7 kHz are shown in Fig. 1. For 4 kHz operation the measured seed intensity falls to near zero intensity at the tube walls, has a full width half maximum (FWHM) of 75% of the tube aperture, and may be depleted by up to 50% in the centre. At 7 kHz where the seed intensity is found to be greatly depleted on axis, the seed radiation forms a thin annulus corresponding to emission occurring within $\sim$3 mm of the tube wall [17].

Using the unfolded resonator approach with an unloaded resonator and measured seed intensity profiles, the divergence characteristics of each of the temporal components of the CVL output are now considered separately.

A. Two-Pass Output (ASE)

The two-pass output consists of seed radiation that reflects once off the high reflector before exiting the unstable resonator past the spot reflector output coupler. As this radiation has not reflected off the spot reflector it is usually called the ASE

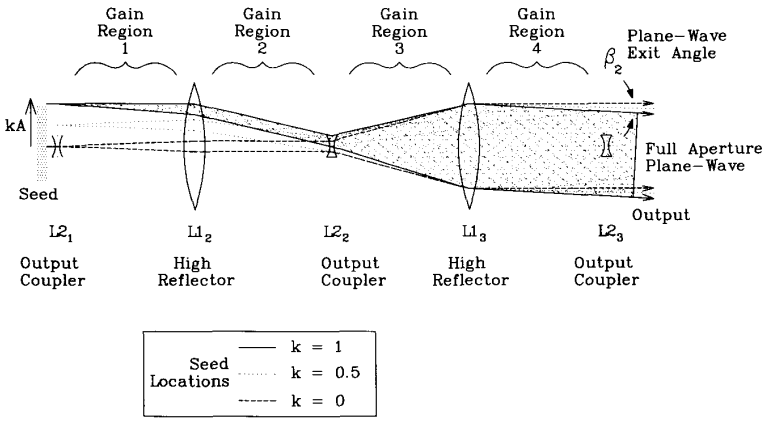

Fig. 2. Examples of ray-paths for spontaneous emission which undergoes four passes through the gain medium before exiting the unfolded resonator. The plane-waves produced by three different seed points are indicated.

(even though the model presented in this paper is based on the observation that all the CVL output can be directly attributed to arising from the amplification of a spontaneous emission seed).

The range of propagation directions for rays from the seed that exit the resonator at the output coupler after reflecting off the high reflector is limited only by the laser tube aspect ratio, and is therefore typically five to ten milliradians. Note that for some CVL operating conditions (where the gain duration is minimum) this component may contain up to half the total CVL output power, but because of its high divergence the two-pass output is not usually considered useful and is often removed from the output using an external spatial filter.

B. Four-Pass Output

Under many operating conditions, the greatest fraction of the CVL output is derived from seed radiation which undergoes just four passes through the gain medium. This output consists of radiation from the seed region (which is located at the output coupler end of the CVL gain volume) which propagates on four transits through the gain medium before exiting the unstable resonator past the spot reflector output coupler having reflected off the spot reflector only once. Fig. 2 shows the propagation of rays from the seed on four passes through the unfolded resonator lensguide. To simplify the analysis, the seed region has been placed initially at the common focus of the resonator mirrors[1] .

The ray matrix [19] for propagation of rays from an arbitrary seed point through the unstable resonator to the output aperture is given by

$$\begin{bmatrix} \alpha_2 \\ \beta_2 \end{bmatrix} = \begin{bmatrix} \dfrac{1}{M} & \dfrac{M^2 d}{M-1} \\ \dfrac{1-M}{M^2 d} & 0 \end{bmatrix} \cdot \begin{bmatrix} \alpha_1 \\ \beta_1 \end{bmatrix} \tag{1}$$

where α and β are the ray heights and propagation angles, d is the resonator mirror separation and M is the cavity magnification. For any arbitrary point on the seed of height ($\alpha_1 = kA\,(0 \le k \le 1, A$ is the tube radius) from the resonator axis, all rays that exit the resonator through the final output aperture have the same final propagation angle given by

$$\beta_2 = kA\frac{1-M}{M^2 d} \tag{2}$$

Thus each seed point gives rise to a plane wave at the output which propagates at an angle β_2 to the resonator axis.

The transverse extent of each plane wave as it exits the unstable resonator depends on the aperturing conditions imposed on the propagation of rays by the finite size of the resonator mirrors and the laser tube itself. It is these aperturing conditions that determine the geometric constraints on propagation of amplified spontaneous emission through the unfolded resonator and thus determine the output divergence. The aperturing conditions are different for on-axis and off-axis resonators and are now considered separately.

1) On-Axis Unstable Resonator: The two principal limiting apertures in the unfolded lensguide are the tube radius (A) and the spot reflector radius (a). Ideally the spot reflector radius is chosen to satisfy a = A/M, which may for example equate to a spot reflector radius of just 0.25 mm for an $M = 50$ unstable resonator and a beam diameter of 25 mm. Due to the difficulty of manufacturing such small spot reflectors, a larger sized spot reflector (typically 1 or 2 mm in diameter) is often used. (Note that even these larger spot reflectors obscure less than 0.2% of the output beam area.)

For the case of the larger than optimum spot reflector diameter (at least twice as large), the only limiting aperture is provided by the laser tube itself, and each point on the seed is found to produce a plane wave occupying the full tube

[1] Translation of the seed disc to somewhere within the first gain medium of the unfolded resonator (where the seed is located in reality) results in the wave derived from each seed point acquiring a radius of curvature of several km, which is essentially indistinguishable from a plane wave. The propagation angle β_2 for each wave is the same whether the seed is located at the common focus or within the first gain region. The choice of seed location at the common focus is therefore a valid simplification.

aperture: $-A \leq \alpha_2 \leq$ A. In this case, the plane-wave beam originating from any given point on the seed disc interacts with the same volume of gain as a beam originating from any other point on the seed disc, this volume being principally determined by the final pass through the laser tube. In this case, assuming radially uniform saturated gain and seed intensity profiles, each seed point gives rise to a plane wave with a uniform intensity profile and with the same fraction of the total four-pass output power. However, each plane-wave exits the resonator at a different propagation angle, that angle being proportional to the lateral displacement of the plane-wave seed point from the resonator axis.

Each plane wave is derived from a single source point and therefore has divergence corresponding to the diffraction limit for plane-wave illumination of a circular aperture. From standard Fraunhofer diffraction theory [20] the FWHM divergence angle for such a wave is given by $\theta_d = 0.515\lambda/A$, where A is the aperture radius.

As each seed point is independent from all other seed points, we can model the total four-pass output as consisting of an *incoherent* sum of diffraction-limited plane waves, where each plane wave propagates at a different angle to the resonator axis. (Note that this corresponds to a k-space description of a diverging or partially coherent beam, where the intensity is examined on time-scales long compared to the CVL temporal coherence width which is typically 10^{-10} s.) We now define the *geometric* divergence θ_g, as the full range of plane-wave exit angles arising from the geometric ray tracing analysis, where

$$\theta_g = 2\frac{(M-1)A}{M^2 d}. \tag{3}$$

In general the four-pass output geometric divergence θ_g, is much larger than that due to diffraction from the final aperture θ_d, the total output divergence therefore being determined principally by the geometric constraints on ray propagation within the unfolded resonator. In such circumstances, to first order the total average FWHM divergence for the four-pass output is given by the geometric divergence θ_g, plus the diffraction divergence θ_d due to the transverse radius A of each of the plane waves

$$\theta = 2\frac{(M-1)A}{M^2 d} + 0.515\frac{\lambda}{A}. \tag{4}$$

Based on the four-pass output description as a distribution of plane-waves with known propagation angles, the far-field intensity profile can also be calculated. The plane-wave from each point on the seed is propagated into the far-field to produce a Bessel function diffraction intensity pattern at the location derived from the plane wave's propagation direction. The far-field diffraction profile from each plane wave is then summed incoherently to produce a component-averaged far-field intensity distribution. This incoherent sum of plane waves represents the average far-field intensity distribution as would be measured by examining the far-field intensity integrated over time-scales of several ns (ie. many times the CVL temporal coherence width)[2] .

A numerically calculated four-pass far-field intensity profile for a CVL (tube diameter 25 mm) operating with an on-axis unstable resonator magnification $M = 26.5$ and mirror separation of 1.8 m, assuming a radially uniform seed profile is given in Fig. 3(a). For this example, the FWHM four-pass divergence is approximately 520 μrad (compared with 525 μrad calculated directly from (4)), and corresponds to 25 times the diffraction-limit.

Where the smaller spot reflector of radius $a = A/M$ is used (corresponding to the size required to produce an intracavity beam of the same radius as the tube radius in the steady-state), the spot reflector imposes a further aperturing condition which restricts the range of exit ray heights (α_2) to

$$-A \leq \alpha_2 \leq A(1-k) \quad (0 \leq k \leq 1). \tag{5}$$

Plane-wave beams which originated from seed points close to the tube wall ($k \approx 1$) therefore have a width reduced to only half of the tube aperture. (Note that diffraction on propagation within the resonator will increase the beam size slightly, but this effect is small except for extremely high magnification resonators which employ very small diameter spot reflectors.) Beams with the greatest angular deviation from the resonator axis have the smallest area, and there is consequently less power in these plane-wave components of the four-pass output. (Assuming uniformly saturated gain, the power contained within each plane wave will be proportional to the volume of gain accessed by that plane wave, and hence is proportional to its exit area.) The effects of a reduced spot reflector radius on the far-field intensity distribution can be seen in Fig. 3(b) which shows the calculated far-field intensity profile for a CVL under the same conditions as in Fig. 3(a) but with a 0.5-mm radius spot reflector. For this example, the reduction in spot reflector radius causes the far-field intensity profile to become peaked on axis and the FWHM divergence is reduced to 440 μrad.

In general the far-field intensity distribution is also modified by the radial variations in the seed intensity. The power contained in the plane-wave produced by each point on the seed is a product of the seed intensity at that point and the volume of gain with which it interacts on propagation through to the output (power extraction is assumed to have no radial variations in this model). For low prf operation where the seed has a relatively uniform radial profile (Fig. 1, 4kHz), the seed intensity does however fall to near zero at the tube walls (with a measured FWHM of 75% of the tube aperture) and has a dip in the middle. This results in a further reduction in FWHM output divergence to approximately 75% of the value calculated from (4). For the previous example with the $M = 26.5$ unstable resonator and a 0.5mm spot reflector radius and using the measured seed intensity profile, the calculated

[2] When examined on sub-nanosecond time-scales, an incoherent sum cannot be assumed, and the relative phases of the different seed points (and their corresponding plane-waves) need to be considered. As the seed consists of random spontaneous emission, the far-field intensity distribution likewise exhibits intrinsically stochastic features, however for the time-scales of concern in the present investigation these intensity variations are averaged out and are therefore not considered here.

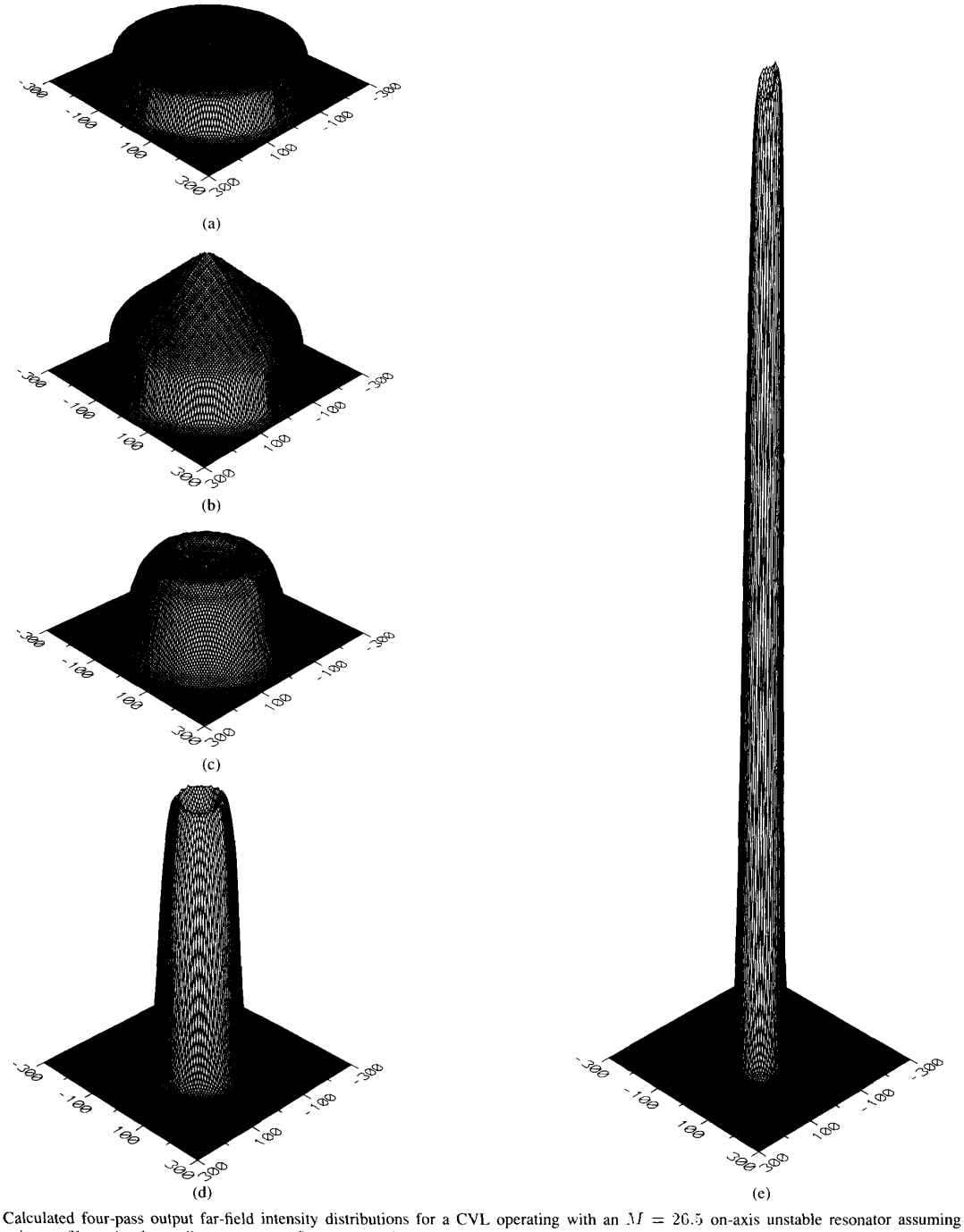

Fig. 3. Calculated four-pass output far-field intensity distributions for a CVL operating with an $M = 26.5$ on-axis unstable resonator assuming uniform seed intensity profile and a large diameter spot reflector (a) and a small diameter spot reflector (b), and for resonator magnifications of 26.5 (c), 50 (d) and 100 (e) using the measured 4 kHz seed profile and small spot reflector. All profiles have the same integrated powers and are plotted with the same relative intensity scale and with the divergence angles marked in micro radians For these modelled far-field profiles, a tube diameter of 25 mm and mirror separation of $\sim$1.8 m have been assumed.

far-field intensity profile (shown in Fig. 3(c)) has only a slight dip in the middle and has a FWHM divergence reduced to 400 μrad.

The effects of changing the resonator magnification can also be seen in Fig. 3, where the expected far-field intensity profiles have also been calculated for resonator magnifications of $M = 50$ (d) and $M = 100$ (e). Note the measured radial seed profile for low prf operation has been used for Fig. 3(c), (d), (e), and equal four-pass output powers have been assumed in all the calculated far-field intensity profiles

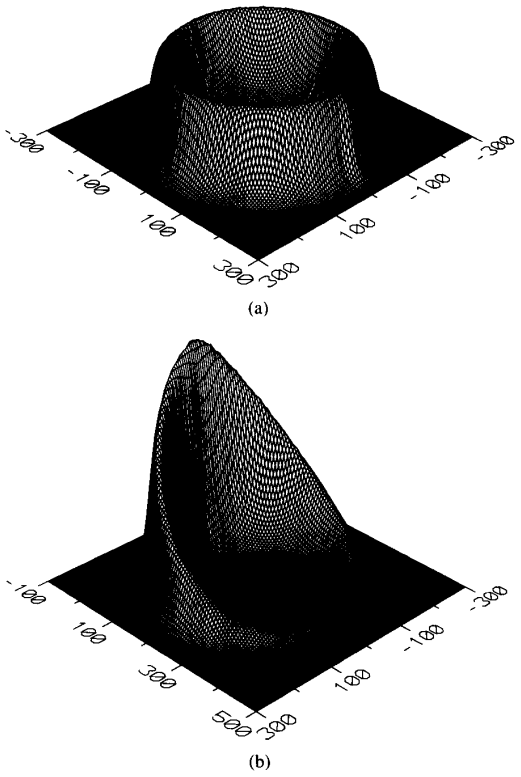

Fig. 4. Calculated four-pass output far-field intensity distributions for a CVL operating with an $M = 26.5$ unstable resonator either on-axis (a) or off-axis (b) and using the measured 7 kHz seed intensity profile.

shown in Fig. 3. By increasing the resonator magnification dramatic increases in far-field intensities may be expected based on these calculations, however it is expected in practice that the higher magnification unstable resonators will produce less output power due to their increased output coupling (i.e., decreased effective reflectivity).

For CVL operating conditions (usually at high prf) where the seed intensity profile is highly annular, the far-field intensity profile of the four-pass output is likewise annular. For example the measured seed profile for 7 kHz operation shown in Fig. 1 corresponds to a thin annulus with a peak corresponding to $k \approx \pm 0.8$. The four-pass output for these operating conditions is therefore modelled as consisting of a sum of full aperture plane waves with propagation directions lying on a cone of angle given by 0.8 times the full angular range of the uniform seed case. Using the measured seed intensity profile for 7 kHz operation shown in Fig. 1, the far-field intensity distribution was calculated as before and is shown in Fig. 4(a) where the same $M = 26.5$ on-axis unstable resonator with the 0.5 mm radius spot reflector is used. Note that extent of the far-field profile is the same for the annular seed as for a uniform seed intensity profile, however the 7 kHz far-field intensity is near zero on-axis. In order to avoid obtaining an annular four-pass output far-field intensity profile from CVL's operating where the seed is highly annular, it is necessary to operate with an off-axis unstable resonator.

2) Off-Axis Unstable Resonators: An off-axis unstable resonator is formed by translating the spot-reflector output coupler to be aligned with the tube wall, the axis of the resonator therefore lies close to the tube wall and the gain is no longer distributed symmetrically about the resonator axis [12].

The aperturing conditions corresponding to propagation of four-pass output rays in the horizontal and vertical planes of a horizontally-displaced off-axis unstable resonator are shown in Fig. 5. In the analysis of the of four-pass output for the on-axis resonator with a spot reflector of radius A/M there was a reduction in output beam size for component plane-wave beams originating from seed radiation near the tube walls. For the off-axis resonator, the spot reflector size can be chosen such that the width (in the horizontal plane) of the four-pass output plane-waves which originated from seed points near the tube wall on the side opposite the resonator axis is reduced to near zero (see Fig. 5(a)). That is, seed radiation from such points does not give rise to any significant four-pass output due to the finite apertures of the resonator mirrors (diffraction and scattering effects are ignored). However, in the vertical plane (shown in Fig. 5(b)) the off-axis resonator displays the same symmetry as for an on-axis resonator, thus in this plane a region of the seed centred on the resonator axis contributes most to the four-pass output.

Off-axis unstable resonators are usually employed for CVL operating conditions where the seed radiation has an annular intensity profile. In this case, one side of the seed annulus consists of seed points displaced too far from the resonator axis to contribute significantly to the four-pass output. It follows that the four-pass output is derived from a crescent shaped seed region as shown in Fig. 5(c). The four-pass output far-field intensity profile therefore also corresponds to a thin crescent, and is thus *highly anisotropic* as can be seen in the calculated far-field profile for an $M = 26.5$ off-axis aligned resonator given in Fig. 4(b). Comparison of Figs. 4(a) and (b) shows that there are two important advantages of off-axis aligned unstable resonators for conditions where the seed is annular. Firstly, there is a significant reduction in divergence (and corresponding increase in peak focal power density) when the same magnification unstable resonator is aligned off-axis rather than on-axis (assuming equal powers in the four-pass components). While the FWHM divergence in the vertical plane is only marginally reduced, in the horizontal plane the off-axis FWHM divergence is approximately one third of the on-axis case. The second major advantage of the off-axis unstable resonator is that the far-field intensity maximum is located at the resonator axis (given by coordinates 0, 0 in Figs. 3 and 4), whereas the on-axis resonator has a minimum intensity on axis in the far-field. Note that the complicated profiles obtained with an annular seed (with either resonator) cannot be accurately characterised using a single dimensionless parameter (such as the FWHM divergence or the transverse coherence radius).

C. Six-Pass Output

The spatial characteristics of the six-pass component of the CVL output may be determined by propagating the four-pass

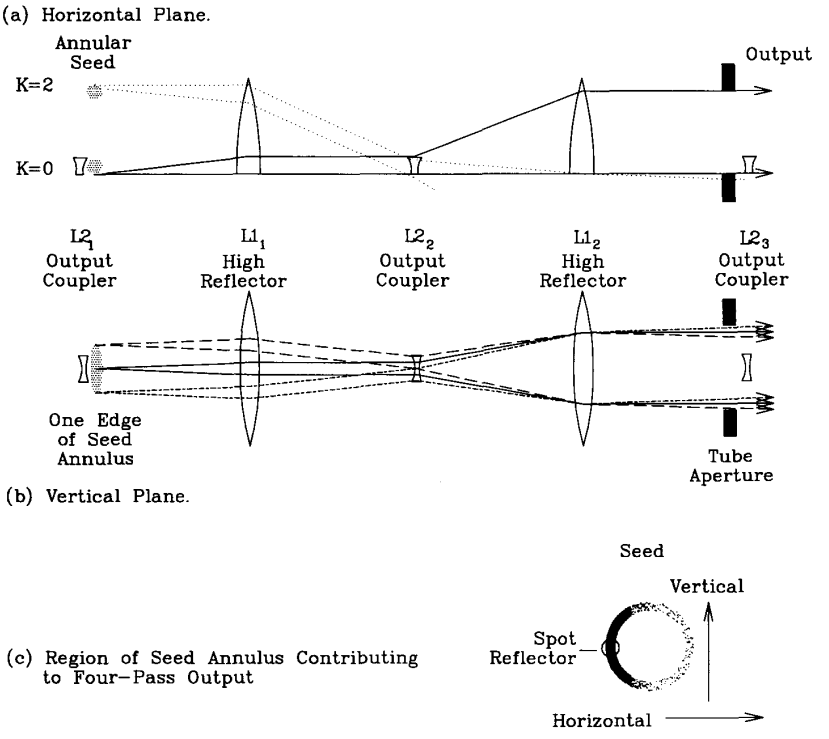

Fig. 5. Off-axis unstable resonator four-pass output ray tracing diagrams. (a) ray-paths in the horizontal plane, (b) ray-paths in the vertical plane, (c) region of seed contributing to high prf off-axis four-pass output.

output on one further complete round trip within the unstable resonator.

Propagation through one complete round trip of an on-axis or off-axis confocal unstable resonator of magnification M is equivalent to passing through an expanding telescope having the same magnification (where the round-trip begins with a reflection off the spot reflector ($L2_2$), as is shown in Fig. 6). Propagation of rays through an expanding telescope of magnification M results in a reduction of the ray angle by a factor of M; thus the geometric divergence of the six-pass output is a factor of M lower than the four-pass output, which for an on axis unstable resonator corresponds to:

$$\theta_g = 2\frac{(M-1)A}{M^3 d}. \tag{6}$$

As before, we must consider the effects of the diffraction divergence of each plane wave in order to evaluate the expected total divergence. For most resonators used in practice, the magnification is such that the six-pass output geometric divergence θ_g is of the same order as that due to diffraction from the final aperture θ_d. In this case the divergence is best determined by calculating the far-field intensity profile using the procedure outlined for calculation of four-pass output far-field profiles.

Calculated far-field intensity profiles for the $M = 16, M = 26$ and for a diffraction-limited top-hat plane wave are given in Fig. 7. Once again it is important to note that these profiles represent the intensity distribution averaged over the duration of the 6-pass output (i.e., many temporal coherence times), thus permitting the plane wave components to be summed incoherently. For all but the lowest magnification ($M = 16$, Fig. 7(a)), the six-pass outputs closely resemble the far-field profile expected from a plane-wave of the same diameter as the CVL beam, complete with diffraction-rings. This means that the effects of the seed intensity profile annularity are no longer resolvable and the off-axis divergence anisotropy is significantly reduced. A further consideration is that only a small fraction of the total four-pass output beam is reflected off the spot reflector output coupler to eventually produce the six-pass output. This fraction corresponds to an area of the beam around the resonator axis, thus it is the spatial information contained within this part of the four-pass output (rather than the total four-pass output) that determines the character of the six-pass output. This tends to reduce, in the six-pass output, the effects resulting from the geometric constraints imposed at the first reflection off the spot reflector ($L2_1$) by the spot-reflector's small size. The six-pass output divergence is therefore largely independent of the spot-reflector size (even for low magnification resonators).

Note that it is the six-pass plane waves' angular deviation from the resonator axis which is reduced by a factor of M from the four-pass value. Thus for the on-axis case, both the four-pass and six-pass far-field intensity maxima are centred on the resonator axis. However, at high prf where the seed is annular, the six-pass output forms a peak in the centre of the four-pass far-field annulus. In contrast, for the off-axis resonator the

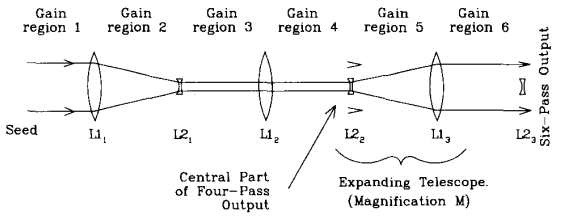

Fig. 6. Six-pass output ray tracing diagram.

four-pass output far-field maximum is already located at the resonator axis, as is the six-pass far-field maximum. Therefore there is no shift in far-field propagation maxima between the four-and six-pass outputs for an off-axis resonator. There will however, be a difference in the *average* propagation direction (defined as the intensity weighted mean of the plane wave propagation directions) between the four-pass and six-pass outputs of an off-axis unstable resonator due to the asymmetry in the far-field profiles.

D. Eight-Pass Output

Using the result that propagation through each round-trip reduces the geometric divergence by a factor of M, the general equation for the geometric divergence of the $(2n)$-pass component can be derived:

$$\theta_g = 2\frac{(M-1)A}{M^n d}. \tag{7}$$

For the eight-pass output the geometric divergence is typically much less than the diffraction divergence from the exit aperture, and thus this component may be described as having 'diffraction-dominated' divergence. However, in practice optical aberrations in the resonator mirrors and laser windows and thermally-induced refractive index fluctuations in the air outside the laser windows reduce the wavefront integrity across the full beam aperture thus distorting the far-field intensity profile and increasing the divergence.

III. Experiment

A one-dimensional imaging system (described in detail in [8]), together with a fast-gated linear diode array detector, was used to record far-field intensity distributions of each temporal component of the CVL pulse from a medium-scale (20 W) laser. The one-dimensional imaging arrangement consisted of a $f = 300$ mm cylindrical focusing lens which produced a line focus, which was then imaged onto a distant detector (Princeton Instruments IRY512) using a second cylindrical lens ($f = 25.4$ mm). A line focus arrangement is ideally matched to linear detection as the fraction of the total CVL output power emitted within any given divergence angle is directly proportional to the corresponding area under measured intensity profile [8]. Dichroic beam splitters were used to select either the green or yellow CVL output before detection. The detector was gated to capture 5 ns time-slices of the far-field intensity distribution from single CVL pulses. Each time-slice therefore corresponds to measuring the time-averaged far-field intensity distribution for a single temporal component of the CVL output.

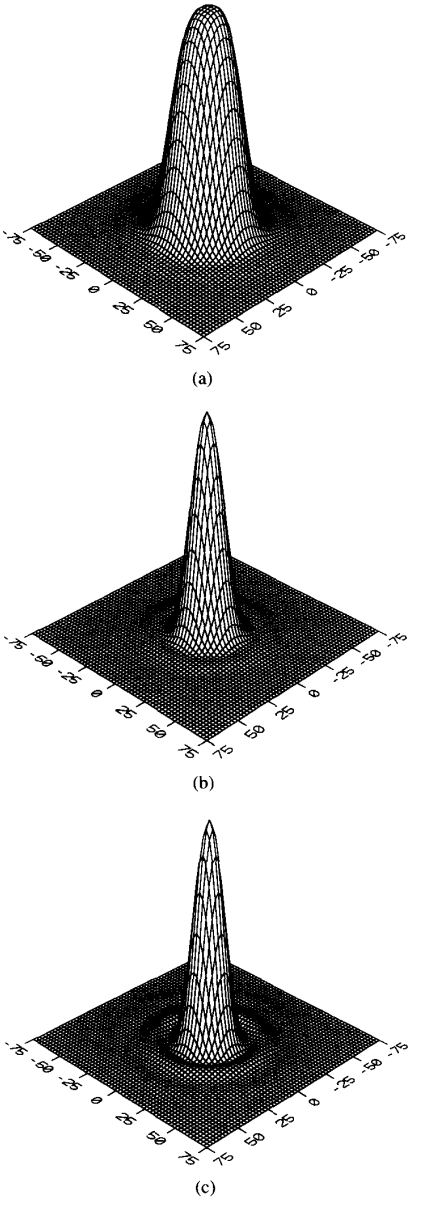

Fig. 7. Calculated six-pass output far-field intensity profiles for a CVL operating with (a) an $M = 16$ and (b) and $M = 26$ on-axis unstable resonator ($d \sim 1.8$ m, tube diameter = 25 mm), and (c) for a 25 mm diameter top-hat plane wave.

A nominally 20 W CVL (active volume 25 mm id, 1 m long) was used for the experiments. The laser was fitted with both on-axis and off-axis confocal unstable resonators consisting of an $R = 4$ m high reflector, and a choice of four spot reflector output couplers. The output couplers were all 2 mm in diameter and had radii of curvature of 246 mm, 151 mm, 80 mm and 40 mm corresponding to resonator magnifications M, of 16, 26.5, 50 and 100. The CVL was operated at pulse repetition

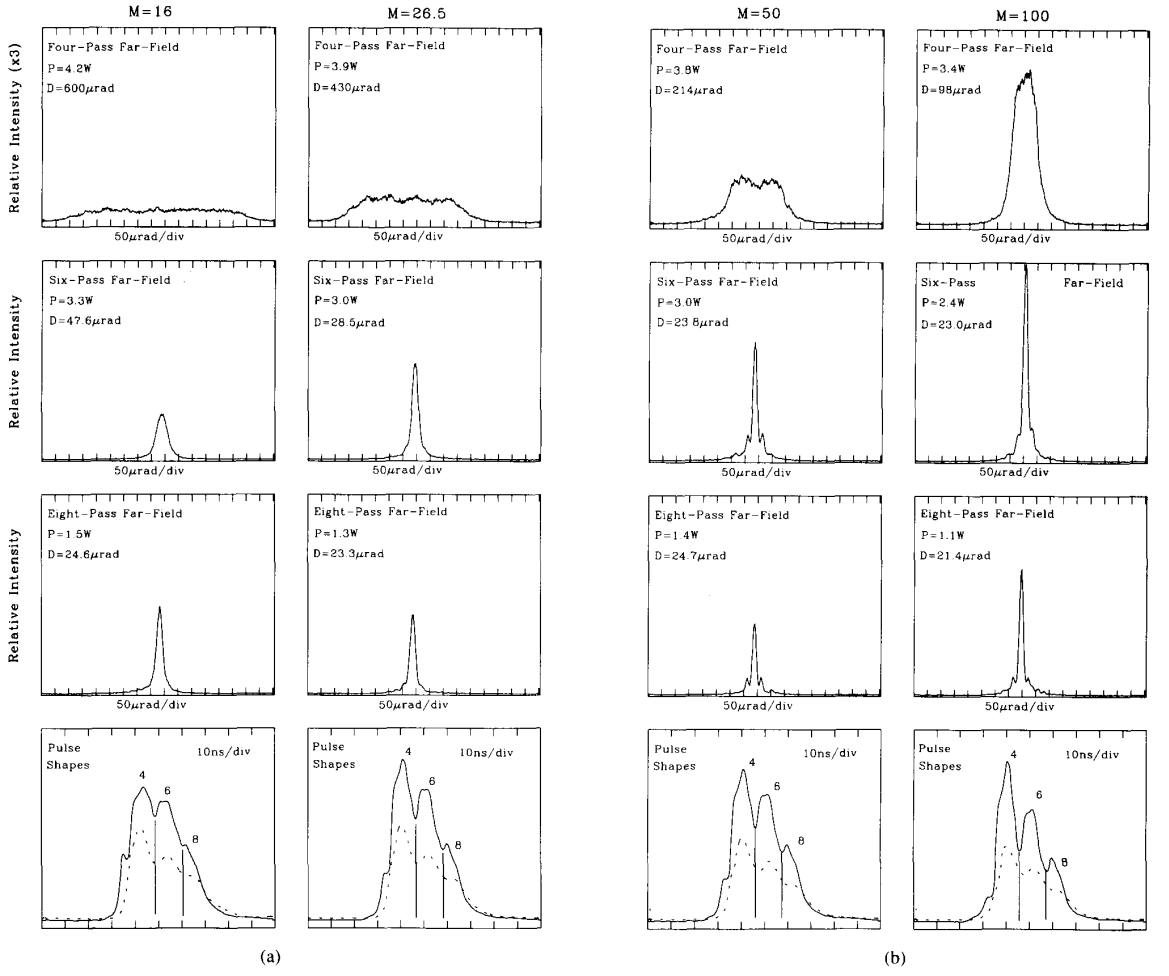

Fig. 8. Measured far-field intensity distributions of the different temporal components of the CVL output for different resonator magnifications and at a prf of 4 kHz. Each component is labelled with its measured multishot FWHM divergence, and green component power. Pulse shapes are also included for the green (solid line) and yellow (dashed line).

frequencies of 4 kHz, and 7 kHz corresponding to the two measured seed profiles of Fig. 1.

A. Low prf

Measured far-field intensity distributions for the different temporal components observed for the CVL operating at 4 kHz prf and with on-axis resonators of magnification 16, 26.5, 50, or 100 are shown in Fig. 8. Only the green profiles are given in Fig. 8 as the yellow output has essentially the same divergence behaviour, but the different yellow components are not as well temporally defined as the green components due to the more complicated spectral turn-on characteristics of the yellow output [17]. Green (and yellow) pulse shapes showing the different temporal components, together with the green powers in each component, are also included in Fig. 8.

The measured profiles display the same features as are in the corresponding calculated far-field profiles, however the measured profiles were formed by cylindrical (line) focusing which for example reduces the visibility of the dip in the middle of the four-pass output profiles. There is also less variation with resonator magnification in peak measured far-field intensity than that for the calculated profiles, this is because the peak 1-D far-field intensity is inversely proportional to the divergence rather than the square of the divergence for 2-D imaging. Diffraction side-lobes arising from the top-hat near field intensity profile are readily observed in the profiles of those outputs with near diffraction-limited divergence.

The measured profiles are not as smooth as the calculated profiles, however the calculated profiles represent an ideal average far-field intensity. In practice there is considerable shot-to-shot variation across the far-field intensity profiles (although the FWHM is relatively constant shot-to-shot), and even more variation within the duration of the four-pass component of a single pulse, as can be determined by examining the temporal characteristics at any point in the four-pass far-field with a fast response photodiode (e.g., Hammamatsu R113U-02) and fast oscilloscope (Tektronix 7104). This demonstrates that the far-field spread in intensity of the four-pass output is principally

due to randomness in the output wavefront (due to partial transverse coherence). The randomness in the wavefront is to be expected as the CVL output effectively consists of multipass amplified spontaneous emission (which is inherently random).

From the profiles of Fig. 8, four-pass FWHM output divergences at 4 kHz prf for the $M = 16, M = 26.5, M = 50$, and $M = 100$ resonators were measured to be 600 μrad, 430 μrad, 214 μrad and 98 μrad respectively. Corresponding theoretical values (derived from (4) modified by the measured seed intensity profile) for the four resonators were 650 μrad, 400 μrad, 220 μrad, and 105 μrad respectively, in excellent agreement with the measured values. These divergences range from 30 times the diffraction limit ($\theta_d = 18.1$ μrad with line imaging) for the $M = 16$ unstable resonator down to six times the diffraction limit for the highest magnification investigated.

Six pass output divergences measured for the four unstable resonators in ascending order of magnification were 47.6 μrad, 28.5 μrad, 23.8 μrad and 23 μrad, and the corresponding theoretically expected values are (from the calculated profiles) 40 μrad, 20.6 μrad, 18.25 μrad and 18.1 μrad respectively. These divergences range from 2.6 times the diffraction-limit for the lowest magnification, to less than 30% greater than the diffraction limit for the highest magnification, representing dramatic increases in beam quality over the corresponding four pass outputs.

The eight-pass outputs had divergences varying from 21.4 μrad to 24.7 μrad, which are approximately 20–30% greater than the theoretical diffraction divergence. However for the $M \geq 26$ resonators, the eight-pass output displayed full transverse coherence. The difference between expected and measured values is most likely due to aberrations in the plano-convex cylindrical lenses used to form the far-field image and errors in determining when the imaging system is accurately aligned to produce the far-field image on the detector array. If we assume that these eight-pass components do indeed have diffraction-limited divergences, then the six-pass divergences may be scaled relative to the eight-pass to determine how they vary from the calculated values. When thus scaled, the six-pass outputs vary by less than 10% from the values determined using the geometric plane-wave propagation model.

B. High prf

Far-field intensity distributions for the three principal temporal components of the output were recorded for the CVL operating at elevated prf (7 kHz) and with both on-axis and off-axis (horizontally displaced) unstable resonators. Results for the $M = 26.5$ unstable resonator are shown in Fig. 9. The divergence was measured in the horizontal and vertical planes separately for the off-axis resonator due to the resonator asymmetry. Again pulse shapes and green component powers were measured and are included in Fig. 9.

The four-pass output far-field intensity profile for the on-axis resonators were annular (following the seed profile) which with the cylindrical imaging arrangement produced two-peaked far-field intensity distributions as is shown for the $M = 26.5$ unstable resonator in Fig. 9. For the $M = 26.5$ resonator the outer FWHM divergence angle was 480 μrad, which is approximately 10% greater than for the same resonator at 4kHz prf. This increase in divergence results from the high prf annular seed intensity profile peaking closer to the tube walls (peak at $r \approx 0.8A$) producing an output divergence approaching the FWHM angle given from (4). Note that the highly annular far-field profile at 7 kHz prf is only fully apparent when two-dimensional imaging is used, as the line focus technique integrates an annular profile in the direction orthogonal to the line focus producing a more filled-in profile as in the example given in Fig. 9. Two dimensional imaging was not used for the divergence measurements presented in this paper as it is not suited to detection with a linear array detector (the effects of wavefront distortion and beam pointing stability make accurate measurements of the divergence characteristics of the diffraction-dominated components very difficult with a linear array detector).

For the off-axis resonator, where the ray trace analysis predicts that only one side of the annular seed contributes to the four-pass output (resulting in the calculated far-field intensity profile given in Fig. 4(b)), the divergence was found experimentally to be strongly anisotropic (Fig. 9). In the vertical plane the FWHM divergence is 47% lower than for the same resonator on-axis, and in the horizontal plane there is a more dramatic reduction in FWHM divergence angle to just 13% of the on-axis value. Using two-dimensional imaging, a crescent shaped far-field intensity distribution is observed corresponding to that predicted from the model. These results demonstrate that there is a significant improvement in the divergence of the four-pass output from an off-axis unstable resonator compared with an on-axis unstable resonator. The improvement in four-pass divergence was found to be critically dependent on the resonator alignment. Changes in the resonator alignment alter the geometric aperturing conditions for propagation of rays from the seed, thus modifying the resultant far-field intensity distribution.

Note that the annular and anisotropic natures of the far-field intensity profile for these components would not be apparent if just a single parameter characterisation such as the FWHM divergence angle, the Strehl ratio [21], the M^2 parameter [22], or the transverse coherence radius [9]–[11] alone were used to characterise the CVL beam quality. For CVL systems, such beam quality parameters are more applicable to characterising the deviation of the near diffraction-limited six-pass and eight-pass components from a pure TEM_{00} gaussian beam. These deviations relate to the influence of wavefront distortions due to air turbulence near the laser windows, non-ideal optical elements, and the top-hat near-field beam profile (which is also modified by the shadow of the spot reflector and the occlusion of the beam due to the liquid copper supply at the bottom of the plasma tube). These effects occur in addition to the divergence features of interest in this paper (i.e., the effects arising from the manner in which the output is formed from an ASE seed).

Six-pass output divergences for both on- and off-axis unstable resonators were found to be up to 40% greater than the diffraction-limit, corresponding to those divergences arising from both diffractive and geometric propagation effects in similar proportion (as was observed at 4 kHz prf). Variations

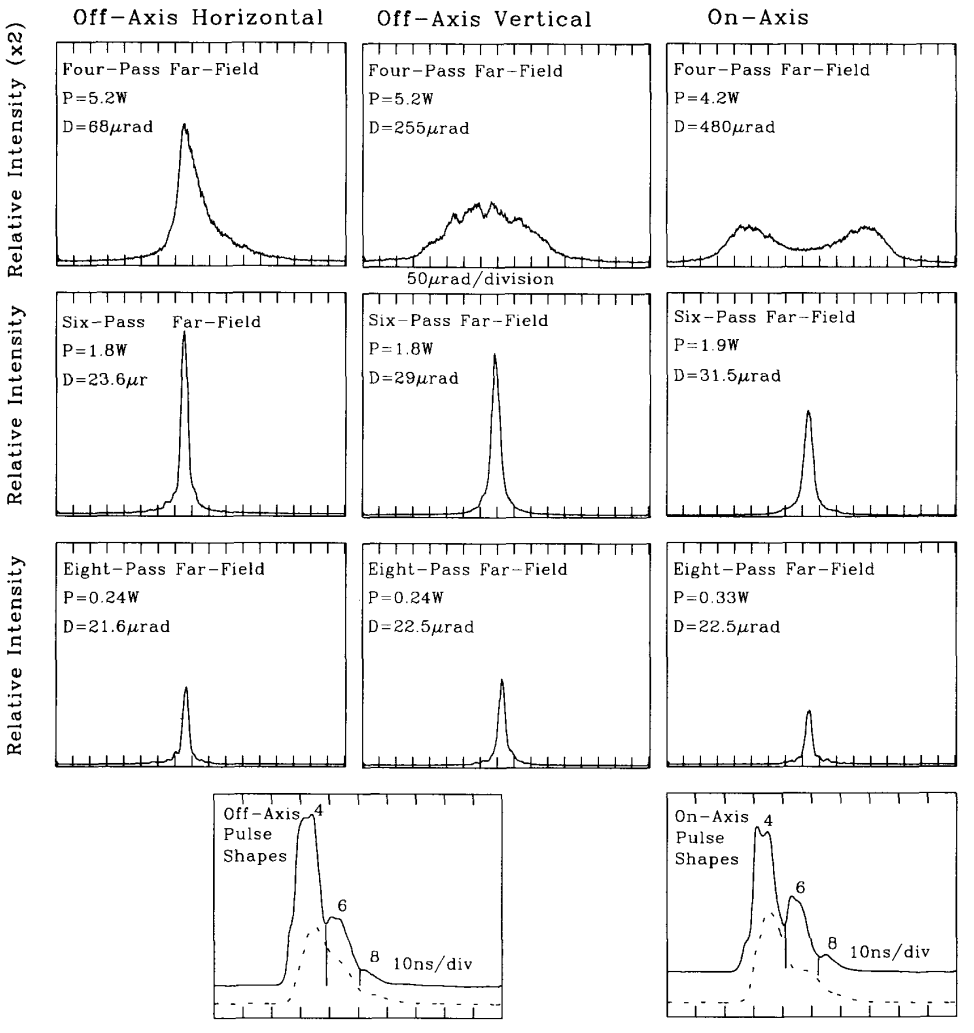

Fig. 9. Measured far-field intensity distributions of the different temporal components of the CVL output at 7 kHz prf with both on-axis and off-axis $M = 26.5$ unstable resonators. The far-field intensity profiles are recorded in both the horizontal and vertical planes separately for the off-axis unstable resonator. Each component is labelled with its multishot FWHM divergence, and green component power. Green (solid line) and yellow (dashed line) pulse shapes are also included.

in resonator axis placement and the seeding geometry (annular vs disc) no longer greatly affect the far-field intensity profiles. However the off-axis unstable resonator does produce a measurable improvement in beam quality over the on-axis case, with the divergence varying from 1.4 times the diffraction limit for on-axis to 1.1 and 1.3 times for the horizontal and vertical planes respectively for the off-axis case. A further observation is that for the on-axis unstable resonator the six-pass output grows from the centre of the annular four-pass far-field intensity distribution, whereas with the off-axis unstable resonator the maximum in the four and six-pass far-field intensity distributions occur at the same point.

C. Component Powers.

The green and yellow pulse shapes were recorded for each resonator and operating condition and are also included in Figs. 8 and 9. From these pulse shapes the power contained in each temporal component of the green outputs was estimated by dividing each pulse into its separate temporal components and comparing their areas (the different components could only be clearly resolved for the green outputs). The component powers are also listed in Figs. 8 and 9. For all resonators and operating conditions the four-pass component had the greatest fraction of the total green output power (up to 5.2 W for $M = 26.5$ on-axis resonator at 7 kHz), and the eight-pass output had the least (just 0.24 W for the $M = 26.5$ on-axis resonator at 7 kHz). The power in any given temporal component varied with resonator magnification being lowest for the highest magnification unstable resonator ($M = 100$), and highest for the lowest magnification resonator ($M = 16$), but was similar for the $M = 26.5$ and $M = 50$ resonators. The reduction in power with increased resonator magnification is

partially offset by a reduction in beam divergence, resulting in a peak power density at focus that increased with resonator magnification. The total green power within a divergence angle of 21 μrad (i.e., within the diffraction-limit) from each resonator at 4 kHz prf was highest for the $M = 50$ resonator which gave 4.4 W, as opposed to 3.6 W for $M = 100$, 2.8 W for $M = 26.5$ and 1.5 W for $M = 16$.

IV. Discussion

The results presented in Section III indicate the great variability in the output divergences and powers obtained for the different temporal components produced from a range of resonator magnifications. While the $M = 100$ unstable resonator offers the lowest pulse-average divergence and lowest divergence for each temporal component, the overall output power obtained with this resonator was the lowest of those investigated; the reduction in power for the higher magnifications being due to the very high round-trip output coupling (given by $1 - 1/M \approx 99.99\%$). The high output coupling obtained for the $M = 100$ unstable resonator also renders that resonator the most susceptible to the formation of parasitic resonators with any external optics. If we consider the power available within the diffraction-limit, then the results at 4 kHz indicate that the $M = 50$ unstable resonator is preferred. The choice of optimum resonator therefore depends on the requirements of the application, for example divergences low enough for pumping of dye lasers can readily be obtained with the $M = 16$ unstable resonator, the very low pulse-average divergences required for applications such as master oscillators and micromachining require the use of the highest practical magnification ($\sim$100), whereas applications such as frequency doubling which requires the greatest power within the diffraction-limit call for the use of unstable resonators with less extreme magnifications ($\sim$50). Note that in circumstances where CVL output with maximum possible beam quality is required extremely high magnification ($M \sim 200$) unstable resonators, or self-filtered unstable resonators, [23] are often preferred, however such resonators typically produce very low output powers.

The results also show that to obtain best beam quality for CVL operating conditions where the gain occurs with relatively uniform radial onset (usually corresponding to low prf operation), conventional on-axis unstable resonators are preferred. For CVL's where the seed is annular an off-axis resonator is best, but the divergence is anisotropic. The plane of minimum divergence for an off-axis resonator (which is that plane containing both the resonator and laser tube axes) can be matched to the requirements of the application; for example in nonlinear frequency conversion in BBO the plane of minimum divergence can be chosen to correspond to the angle tuning plane [2]. If the application is such that an anisotropic divergence cannot be tolerated, the on-axis resonator with its radial symmetry is required.

For the CVL operating at higher prfs of 10 kHz and 14 kHz the pulse is shortened to the extent that the four-pass output becomes the dominant component of the total CVL output. In this case the off-axis resonator gives significantly lower pulse-average beam divergence than for the same resonator on-axis; for these situations the strong radial variations in initial gain actually work to our advantage. However, the highest pulse average beam quality is always obtained when the CVL is operating at low prf where the gain duration is at its maximum. Techniques to modify the seed intensity profile may be employed to further tailor the evolution of output beam quality [24].

It may at first sight appear that an off-axis resonator is to be preferred even in the absence of radial gain variations; however, the resulting divergence is anisotropic and the six-pass output far-field intensity distribution peaks at a point corresponding to one side of the four-pass far-field intensity distribution. This means that the off-axis output is potentially less useful than the output obtained from an on-axis unstable resonator for applications which require a high degree of symmetry in the far-field intensity distribution.

V. Conclusion

Detailed measurements of the evolution of divergence for a copper vapor laser operating with a variety of unstable resonators have shown that the CVL output consists several temporally-resolved components, each having markedly different divergence characteristics. The first component (after the normally unusable ASE) which corresponds to spontaneous emission which has made just four passes through the gain medium, has a divergence strongly influenced by the resonator magnification and radial variations in the initial CVL gain. Subsequent components for the high magnification resonators investigated were found to have divergence more dominated by the effects of diffraction from the final laser aperture. An off-axis resonator was shown to produce an anisotropically diverging output which had substantially lower divergence in one plane than the equivalent on-axis resonator.

It was found that the spatial characteristics of the CVL output can be accurately determined from the geometric constraints imposed on the propagation of an initial burst of spontaneous emission ("the seed") on repeated round-trips within the unstable resonator. This formalism resulted in a description of the diverging CVL beam in terms of a sum of plane-wave components where each plane-wave component propagates at a different angle. The angular distribution and relative intensities of the plane-wave components were determined based on the spatial characteristics of the initial gain (and hence corresponding seed intensity) and the volume of gain accessed by each component. Far-field intensity distributions could therefore be predicted with excellent quantitative agreement with far-field profiles measured experimentally. This approach can be applied to any CVL gain distribution and resonator configuration, and is also applicable to any high gain large volume pulsed laser system such as an excimer laser. The plane-wave description also enables the spatial characteristics of the CVL output to be accurately determined after propagation through any arbitrary optical system and hence greatly aids optical design.

ACKNOWLEDGMENT

The author would like to thank D. Brown and J. Piper for many helpful discussions.

REFERENCES

[1] R. Kupfer and H. W. Bergmann, "Materials processing with copper vapor lasers," *Opto Electrinik Magazin*, vol 6, pp. 49–60, 1990.
[2] D. W. Coutts and J. A. Piper, "One watt average power by second harmonic and sum frequency generation from a single medium scale copper vapor laser," *IEEE J. Quantum Electron.*, vol. 28, pp. 1761–1764, 1992.
[3] M. R. H. Knowles and C. E. Webb, "Efficient high-power copper-vapor-laser-pumped Ti : Al_2O_3 laser," *Opt. Lett.*, vol. 18, pp. 607–609, 1993.
[4] K. I. Zemskov, A. A. Isaev, M. A. Kazaryan, G. G. Petrash, and S. G. Rautian, "Use of unstable resonators in achieving the diffraction divergence of the radiation emitted from high-gain pulsed gas lasers," *Sov. J. Quantum Electron.*, vol. 4, pp. 474–477, 1974.
[5] R. S. Hargrove, R. Grove, and T. Kan, "Copper vapor laser unstable resonator oscillator and oscillator-amplifier characteristics," *IEEE J. Quantum Electron.*, vol. QE-16, pp. 1108–1113, 1980.
[6] V. P. Belyaev, V. V. Zubov, A. A. Isaev, N. A. Lyabin, Yu. F. Sobolev, and A. D. Chursin, "Spatial, temporal, and energy characteristics of copper vapor laser radiation," *Sov. J. Quantum Electron.*, vol. 15, pp. 40–44, 1985.
[7] M. Amit, S. Lavi, G. Erez, and E. Miron, "Temporal and spatial properties of an oscillator-amplifier copper vapor laser," *Optics Commun.*, vol. 62, pp. 110–114, 1987.
[8] D. W. Coutts, D. J. W. Brown, and J. A. Piper, "Measurements of the divergence evolution of a copper vapor laser output using a cylindrical imaging technique," *Appl. Opt.*, vol. 32, pp. 2058–2061, 1993.
[9] T. G. M. Freegarde, "Efficient high average power harmonic generation using copper vapor lasers," *Dig. Tech. Pap.*, CLEO '90, paper CThK3, 1990.
[10] D. W. Coutts, M. D. Ainsworth, and J. A. Piper, "Observation of the temporal evolution of transverse coherence in copper vapor lasers," *Optics Commun.*, vol. 87, pp. 245–248, 1992.
[11] T. Omatsu, K. Kuroda, and T. Takase, "Time-resolved measurement of spatial coherence of a copper vapor laser beam using a reversal shear interferometer," *Optics Commun.*, vol. 87, pp. 278–286, 1992.
[12] A. J. Kearsley, G. A. Naylor, and R. R. Lewis, "Optimization of resonator design for large-volume short-pulse copper vapor lasers," *Dig. Tech. Pap.*, CLEO'87, paper MG1, 1987.
[13] D. W. Coutts, M. D. Ainsworth, and J. A. Piper, "Enhanced efficiency of uv second harmonic and sum frequency generation from copper vapor lasers," *IEEE J. Quantum Electron.*, vol. 26, pp. 1555–1558, 1990.
[14] A. A. Isaev, M. A. Kazaryan, G. G. Petrash, and S. G. Rautian, "Converging beams in unstable telescopic resonators," *Sov. J. Quantum Electron.*, vol. 4, pp. 761–766, 1974.
[15] Yu. A. Anan'ev, "Establishment of oscillations in unstable resonator," *Sov. J. Quantum Electron.*, vol. 5, pp. 615–617, 1975.
[16] A. A. Isaev, M. A. Kazaryan, G. G. Petrash, S. G. Rautian, and A. M. Shalagin, "Shaping the output beam in a pulsed gas laser with an unstable resonator," *Sov. J. Quantum Electron.*, vol. 7, pp. 746–752, 1977.
[17] D. W. Coutts and D. J. W. Brown, "Establishment of oscillations in a copper vapor laser," *Appl. Opt.*, 1994, in press.
[18] J. M. Eggleston, "Theory of output beam divergence in unstable resonators," *IEEE J. Quantum Electron.*, vol. 24, pp. 1302–1311, 1988.
[19] A. E. Siegman, Lasers, University Science Books, 1986, p. 581.
[20] M. Born and E. Wolf, *Principles of Optics*. Oxford: Pergamon Press, 1980, p. 417.
[21] ——, *Principles of Optics*. Oxford: Pergamon Press, 1980, p. 462.
[22] T. F. Johnston, Jr. "M^2 concept characterizes beam quality," *Laser Focus World*, pp. 173–183, May 1993.
[23] R. Pini, R. Salimbeni, G. Toci, and M. Vannini, "High efficiency diffraction limited operation of a copper vapor laser," *Opt. Commun.*, vol. 81, pp. 138–143, 1991.
[24] M. J. Withford, D. J. W. Brown, D. W. Coutts, and J. A. Piper, "Increased efficiency of high beam quality extraction from a copper vapor laser with H_2Ne admixtures," *Dig. Tech. Pap.*, CLEO'94, paper CFD3, 1994.

David W. Coutts (M'94) was born in Palmerston North, New Zealand, on January 9, 1966. He received the B.Sc. (Hons.) degree from Massey University, Palmerston North, New Zealand in 1987, and the Ph.D. degree from Macquarie University, Sydney, Australia in 1992. His dissertation research involved investigations of beam quality and nonlinear frequency conversion of copper vapor lasers.

In 1992, he took up the post of a Macquarie University Research Fellow in the Centre for Lasers and Applications. Areas of activity include: investigation of optical characteristics (including beam quality, and gain characteristics) of pulsed metal vapor laser oscillator and oscillator/amplifier systems; nonlinear frequency conversion of these lasers (including multistage conversion schemes and power scaling of second-harmonic conversion from copper vapor lasers); and fluorescence conversion techniques (including dye and solid-state lasers).